



Enhancing variability in fibrous structures via geometric modifications of breaker plates in high-moisture extrusion of meat analogues

Laurids Pernice^{*}, Désirée Röhrich, Volker Gaukel, Nico Leister

Karlsruhe Institute of Technology (KIT), Department of Chemical and Process Engineering, Food Process Engineering, 76131, Karlsruhe, Germany

ARTICLE INFO

Keywords:

Meat analogue
Breaker plate
Protein structuring
Elongational flow
Fibrous structure
Macro structure

ABSTRACT

The growing shift away from meat products is a key factor in fighting climate change. High-moisture extrusion (HME) is particularly promising in the production of meat analogues due to its capability to create fiber-like structures that mimic meat textures. However, opportunities remain for diversification to use the full potential of HME. This study highlights the potential of using breaker plates in HME to enhance the versatility of creating fibrous structures and tailoring the mechanical properties of meat analogues. For soy protein isolate, the influence of various breaker plate geometries on the development of fibrous structures is investigated, regarding hole diameter (1–2 mm), hole count (10–14), and channel length (2–4 mm). Tensile tests were conducted in transversal and longitudinal direction to obtain the anisotropy index of the extruded samples. To visualize the fibrous structure, cryo imaging and visual examination of open samples were carried out. Results reveal that breaker plates introduce a secondary structure (parallel strands) overlaying the parabolic primary structure. Achievable anisotropy (1.5–6.5) exceeded the values usually achieved in conventional extrusion. Breaker plate design affected secondary structure formation substantially. Larger hole diameters produced thicker strands with reduced anisotropy (2.9–1.5). Increasing hole number raised anisotropy (1.5–6.4) by altering strand cross-sectional shape and size, accompanied by decreased rupture tension in all directions. Extending flow channels stabilized structural properties against mass flow variations. Thus, we demonstrated that using breaker plates is capable to introduce an additional structural level, allowing for greater variability in mechanical properties.

1. Introduction

The rapid progression of anthropogenic climate change is increasingly threatening the habitats of both humans and other living beings (IPCC, 2023). A significant driver of climate change is the substantial rise in per capita consumption of animal meat over the past decades (Parlasca and Qaim, 2022). However, large segments of the population are unwilling to sacrifice the sensory properties (texture, taste and odor) of meat products (Hoek et al., 2011; Leland et al., 2022). This dilemma has initiated a wide range of research topics aimed at facilitating the development of palatable meat alternatives (Lee et al., 2023). A particular industrial focus is on mimicking the textural properties of animal meat and meat products. While products such as sausages, burger patties, and nuggets require certain levels of firmness, elasticity, and juiciness (Pematilleke et al., 2022), they do not need the large scale anisotropic structure and fibrousness of animal meat. The need for such structures is repeatedly stated for replicating less processed meat products such as shredded meat or whole cut products like roast slices

(Mateen et al., 2023; Wittek et al., 2021a,b; Zink et al., 2023). The extrusion process is the core of the most important industrial manufacturing methods for meat substitute products. Here, in the screw section, the protein-rich raw materials are mixed with water and potentially other additives and plasticized through thermomechanical stress. In the die section, structuring and solidification into a meat substitute product takes place. Specifically, through high moisture extrusion processes (HME) with water contents of 40–80 %, high moisture extruded meat analogues (HMMA) with highly anisotropic, aligned structures, approximating animal meat fibers can be produced (van der Sman and van der Goot, 2023). Using a cooling die, the temperature of the protein-rich mixture is lowered upon exit from the screw section, thus suppressing expansion (Bouvier and Campanella, 2014). As a result, the extrudate shows a dense and firm consistency with a lamellar structure anisotropically aligned along a parabolic shape in the flow direction across the cross-section of the flow channel (Osen et al., 2014). Several hypotheses regarding the underlying structuring mechanisms are discussed in the literature, operating on different size scales

^{*} Corresponding author.

E-mail address: laurids.ernice@kit.edu (L. Pernice).

<https://doi.org/10.1016/j.jfoodeng.2025.112602>

Received 8 February 2025; Received in revised form 24 March 2025; Accepted 4 April 2025

Available online 10 April 2025

0260-8774/© 2025 The Authors. Published by Elsevier Ltd. This is an open access article under the CC BY license (<http://creativecommons.org/licenses/by/4.0/>).

within the extrudate (van der Sman and van der Goot, 2023). On a molecular level Akdogan (1999) describes the structuring through the folding of individual protein macromolecules and their alignment along the flow direction. In contrast Guan et al. (2024) state, that protein clusters form with diameters of approximately 40 nm and lengths greater than 400 nm while the proteins themselves of about 9 nm remain undeformed. On a larger scale Tolstoguzov (1993) presents a theory pointing to phase separation between incompatible biopolymers. Through shear and elongational stresses these multiphase systems are thought to be deformed into the before mentioned parabolic shapes (Grabowska et al., 2014; Krintiras et al., 2015; Wittek et al., 2021a,b). On the basis of that van der Sman and van der Goot (2023) also highlight the syneresis of poorly bound water due to increasing cross-linking of proteins in the solidifying network. Another mechanism of structure formation proposes gel fracture resulting from temperature depending solidification and velocity gradients (Guan et al., 2024; Sägeser et al., 2025).

In all the above mentioned hypotheses, the flow and temperature profiles after the screw section have a central role in the formation of structure. Wittek et al. (2021) describe elongation flow conditions in the transition zone between the screw section and the die section as a crucial factor for structure formation. Similarly, Zhang et al. (2019) identify structure formation happening before the cooling die. The impact of shear and elongation flow on structure formation is furthermore identified for polymeric extrusion technology. In this context droplet blast and filament formation of dispersed polymeric system was investigated under extrusion conditions by Sakellariades and McHugh (1987). Arrigo et al. (2021) highlight the impact of elongation flow on product properties for systems as homogenous polymers and immiscible polymer blends in the context of industrially relevant applications such as film blowing and fiber spinning. Opposed to Wittek et al. (2021), Guyony et al. (2022) point out the length of the cooling die as the most impactful factor in the development of anisotropic structures. However, it remains unclear whether the varying cooling conditions due to the different die lengths had an impact, considering that the temperature profile has a significant influence on structure formation (Kaunisto et al., 2024; Sandoval Murillo et al., 2019). Also, tests in a high temperature shear cell have shown, that the introduction of shear during cooling affects structure formation (Kölmann et al., 2023). Sägeser et al. (2025) highlight the influence of temperature on flow conditions and resulting gel fracture.

Consequently there is significant potential in designing the transition zone and initial die section, as these play a major role in varying flow conditions, such as elongational and shear flow, as well as cooling. Wagner et al. (2024) varied the height-to-width ratio of the flow cross-section of the cooling nozzle to study the effects on heat transfer on mechanical properties. In a patent Pibarot et al. (2020) presented a special designed transition zone for producing injectable meat analogues with a loose structure. Snel et al. (2022) developed a complex setup with a rotating cooling die to decouple shear rate from mass flow but found little influence of rotation speed on fibrousness and mechanical properties.

Well established in extrusion technology, breaker plates are widely used after the screw section to smooth pressure and flow profiles and sieve out large particles (Akdogan, 1999; van der Sman and van der Goot, 2023). The relevance for extrusion of HMMA is stated with respect to pressure and flow homogenization as well as alignment of protein aggregates (Sengar et al., 2023). With regard to the role of elongational flow on the structure alignment (Wittek et al., 2021a,b), we believe that the whole potential of using breaker plates in HME for product design of HMMA is still to be fully explored. Moreover, on a macro scale, parallel protein strands can be produced by incorporating breaker plates into the extrusion process, as recently demonstrated by Zheng et al. (2024). However, a systematic investigation regarding the impact of using different geometric specifications of breaker plates on structure and mechanical properties is still lacking.

This study focuses on investigating the impact of different geometric specifications of breaker plates on the mechanical properties and structure of extruded samples, using soy protein isolate (SPI) as a well-known, nonreactive model system (Wittek et al., 2021a,b). By variation of hole number, the effects of changed flow area ratios and the resulting elongational flow effects between the breaker plate and the cooling die could be examined. Additionally, the thickness of the breaker plate, thereby altering residence time and the development of the flow profile, was investigated. By altering the hole diameters of the breaker plates, we explored the possibility of creating parallel protein strands of different dimensions and thereby contributing to a new path for product design.

2. Material and methods

2.1. Materials

Soy protein isolate (90 % protein content, d.b.) (SPI) with a moisture content of less than 6 % was supplied by Solae LLC (St. Louis, MO, USA). Tap water was used during extrusion runs. For the pre trials, vital wheat gluten (WG) by Kröner Stärke (Ibbenbüren, Germany) with a moisture of less than 8 % was added to SPI, to form protein mixtures.

2.2. Breaker plate geometries

The breaker plate geometries used in the extrusion trials were fabricated from stainless steel in the institute's own workshop. An exemplary representation of the used breaker plates is given in Fig. 1. Cylindrical holes were systematically arranged across the cross-section of the cooling die's flow cross-section (stadium shape) for uniform distance between them. All holes in the breaker plate had the same diameter, to ensure homogenous material flow. The varied geometric parameters included hole diameter d_h , breaker plate length l_c and the flow area ratio (FAR). FAR is defined in equation (1) with A_b being the cumulative flow area of the breaker plate holes and A_c the flow area of the adapter and cooling die cross section

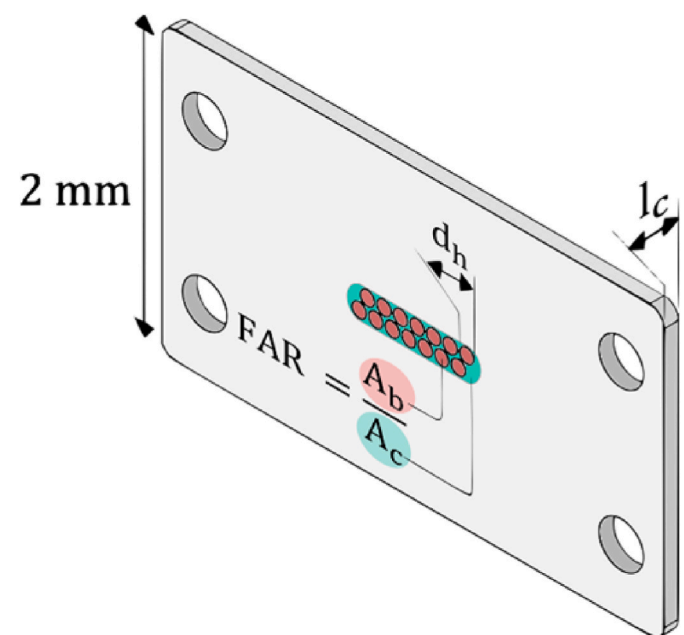


Fig. 1. Schematic representation of an exemplary breaker plate used in the extrusion process, illustrating the hole diameter d_h , channel length l_c , and the flow area ratio FAR, defined as the quotient of the breaker plate's flow area (red) and the adapter flow area (green).

$$FAR = \frac{A_b}{A_c} \quad (1)$$

The values of the varied and constant geometric specifications of the breaker plates are listed in Table 1. For the control, no breaker plate was used. It is therefore not listed in Table 1. For breaker plate A1, the holes are arranged in three rows, whereas all other plates have them in two.

2.3. Extrusion trials

The extrusion experiments were conducted using a co-rotating twin-screw extruder ("Process 11", ThermoFisher Scientific Inc., Waltham, MA, USA) with a length to diameter (L/D) ratio of 40 and a screw diameter of 11 mm. The screw section of the extruder is divided into eight barrels with independent temperature control in the last seven barrels. Solids were fed volumetrically into the first barrel (Brabender Technology GmbH, Duisburg, Germany), while water was dosed into the third barrel using a peristaltic pump ("Masterflex L/S", Cole Parmer, Vernon Hills, IL, USA).

Following the screw section, a 32 mm long heatable adapter narrows the flow cross-section and cross-section shape from that of the screw section (two-overlapping-circles-shape) to that of the cooling die (stadium-shape). The changing shape of the flow cross-section can be quantified by the hydraulic diameter, which is 13.2 for the end of the screw section and 6.8 for the beginning of the cooling die. A visualization of the adapters flow volume is given in figure. A1. As depicted in Fig. 2, the breaker plate was positioned between the adapter and the subsequent cooling die. For the variation of each geometry specifying parameters of the breaker plate (d_h , FAR and l_c) in the main trials, the other two parameters were kept constant.

The flow channel of the cooling die measured 125 mm in length, 19 mm in width, and 4 mm in height. The temperature T_{melt} in the die was controlled using a water-cooled process circulator ("Presto Plus LH 47", Julabo GmbH, Seelbach, Germany). To mitigate the thermal impact of the cooling die on the breaker plate, a PTFE isolation layer was positioned in between (not shown in Fig. 2).

In all extrusion experiments for the process parameters were kept as constant as possible. The screw configuration, visible in Fig. 3, was applied with a screw speed of 600 rpm. The water content of 0.56 neglecting the moisture of the powder and total mass flow of 0.7 kg/h

was also kept constant. For selected samples a mass flow of 1.6 kg/h was chosen. While SPI was used for the main trials, varied SPI to WG ratios (100/0; 70/30; 60/40; 0/100) were used as the protein source for the pre-trials. The temperature in the first five barrels has not been varied during the different trials and were set to 30, 50, 70, 90, 120 °C respectively. The set temperatures in the last two barrels, as well as the set temperature of the adapter, were adjusted iteratively to achieve material temperatures, measured in the adapter of 150 °C for all trials. This way, slight changes in the residence time through the changes in die pressure were compensated. The temperature of the cooling die was set to 40 °C and kept constant throughout all extrusion trials. The material temperature was measured in the adapter.

To show, that extrusion with breaker plates is a viable tool for structurization of HMMA, in a proof of concept we extruded mixtures of varied SPI to WG ratios (100/0; 70/30; 60/40; 0/100) exemplarily with breaker plate A1.

Extrudate samples were taken 5 min after achieving stationary state in material temperature and pressure. All samples were vacuumed immediately after exit, frozen and stored at −18 °C until analysis.

2.4. Rupture analysis

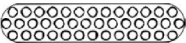






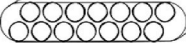
For the optical analysis of anisotropy via rupture inducing technique frozen and vacuumed samples were left at room temperature for complete thawing and room temperature adjustment. For the rupture analysis the samples were slightly cut, held on the cut locations and then teared open completely to reveal the anisotropic structure and the photograph was taken. This is illustrated in Fig. 4A on the left side.

2.5. Cryo imaging

For detailed analysis of the anisotropic structure cryo cutting provided insights into the lamellar structure and fiber orientation with a cryo microtome (Leica Biosystems GmbH, Nussloch, Germany). A method earlier described by Wittek et al. (2021a; 2021b) was used with slight modifications. First the locations of interest were cut to size in frozen state as can be seen schematically in Fig. 4B on the right. They then were covered with a sectioning medium („FSC 22 Frozen Section Media“, Leica Biosystems GmbH, Nussloch, Germany) and placed on a sample holder which was cooled to −20 °C. The cooling room

Table 1

Listing of the geometric specifications of the breaker plates used in the extrusion trials. Here, d_h denotes the hole diameter, FAR the flow area ratio, and l_c the breaker plate thickness.

Varied parameter	Variation		Constant parameters
hole diameter (d_h)	A1		$l_c = 2 \text{ mm}$
	B1		$FAR = 0.4$
	C1		
flow area ratio (FAR)	C1		$l_c = 2 \text{ mm}$
	C2		$d_h = 2 \text{ mm}$
	C3		
breaker plate thickness (l_c)	C3		$d_h = 2 \text{ mm}$
	C3_2		$FAR = 0.6$

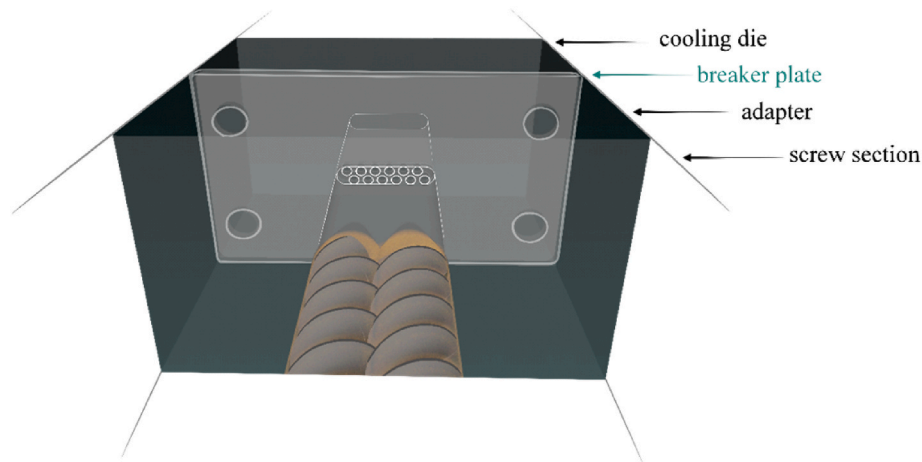


Fig. 2. Schematic showing the positioning of the breaker plate within the relevant section of the extruder, specifically located between the adapter and the cooling die.

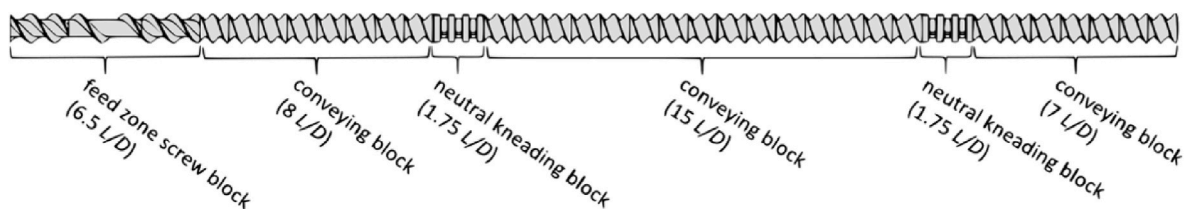


Fig. 3. Schematic representation detailing the specific quantities and positioning of the screw elements utilized in the extrusion trials.

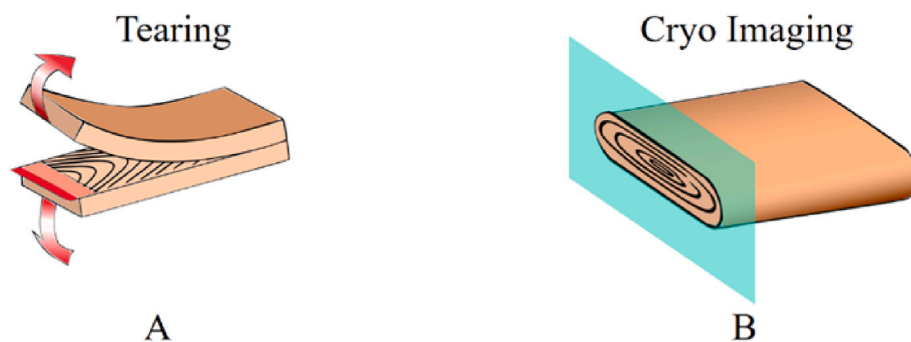


Fig. 4. Visualization of sample preparation procedure for tearing (A) and cryo imaging (B) analysis.

temperature was set to -24°C . Slices of $40\ \mu\text{m}$ were cut from the surface of the sample using a sectioning blade, till the sections of interest were revealed as smooth surface. Then a photograph of this surface was taken.

2.6. Analysis of mechanical properties

To assess the mechanical properties related to texture perception, tensile testing was applied to all the samples using a texture analyzer (zwickiLine Z2.5 TS, Zwick & Roell, Ulm, Germany). To quantify the tensile strength and the resulting anisotropy, samples were investigated parallel and perpendicular to the extrusion direction via tensile testing, as can be seen in Fig. 5. With definition of the cross-sectional area, the transversal and longitudinal rupture tension can be calculated. Hereby, the rupture tension is the maximum tension before the first macroscopic rupture occurs.

To measure the rupture force in both directions, the extrudate was stamped for transversal strength testing using a 10 mm stamp and a 6 mm stamp for longitudinal strength testing to create a defined location of rupture. For testing the strength in longitudinal direction, the

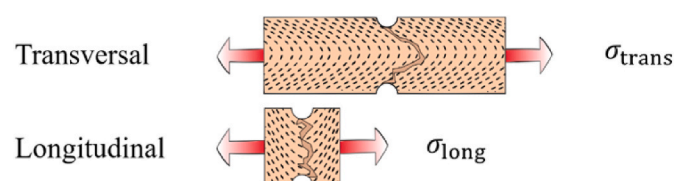


Fig. 5. Visualization of the procedure for analysis of mechanical properties for transversal and longitudinal strength.

extrudate could not be clamped due to its small dimensions (19 mm). It was therefore glued to a piece of wood on both ends using instant adhesive (UHU GmbH und Co. KG, Bühl, Germany) as can be seen in the supporting information in figure A2. This wooden pieces then were clamped in the testing geometry („type 8201“, Zwick & Roell, Ulm, Germany). For tensile tests in transversal direction the extrudate was clamped directly in the testing geometry.

The sample was stretched at a speed of 1 mm/s till rupture and the

maximum force was measured. The stress was calculated using the cross-sectional area of predicted rupture. Using the maximum stress in transversal (σ_{trans}) and longitudinal (σ_{long}) direction, the anisotropy index AI was calculated as follows:

$$AI = \frac{\sigma_{\text{trans}}}{\sigma_{\text{long}}} \quad (2)$$

Here, stress is calculated as

$$\sigma = \frac{F}{A} \quad (3)$$

where F is the maximum force in each direction and A the surface between the opposite stamps.

2.7. Statistical analysis

OriginPro 2023 was used for statistical analysis. For tensile testing, the data are expressed as mean values and standard deviations from six measurements. Differences between samples from the extrusion trials were evaluated separately for transversal and longitudinal rupture tension by one-way ANOVA applying Turkey test at a significance level of $p < 0.05$.

3. Results and discussion

In pre-trials (section 3.1), we showcased the viability of structuring SPI-WG mixtures via extrusion processing with a breaker plate. In the main trials, the influence of various breaker plate geometries on the formation of the parabolic structure (primary structure) and the breaker plate-induced parallel strands (secondary structure) has been investigated. This investigation focused on the visual and mechanical properties of the extrudates. The tested geometries differ in terms of hole diameter (section 3.2), hole number (section 3.3), and channel length (section 3.4).

3.1. Influence of WG content in SPI-WG mixtures

In the pre trials, four WG-SPI mixtures with varying WG content (0 %, 30 %, 40 %, and 100 %) were extruded using breaker plate A1. Additionally, a control sample with 0 % WG was extruded without a breaker plate. Torn open samples are depicted in Fig. 6, with WG content increasing from left to right. It is evident that the control sample exhibits a parabolic shape (primary structure), which is characteristic of conventionally extruded HMMA. For all samples extruded with breaker plate A1, parallel strands are observed, referred to as secondary structure. In the case of 100 % WG, this structure is significantly less pronounced, displaying an overall brittle and soft appearance. The

reduction in hardness of HMMA with rising WG to SPI ratio was also observed earlier by Jiang et al. (2024). Furthermore, for the 0 % WG sample extruded with breaker plate, the parabolic structure remained visible. A similar superimposition of primary and the secondary structure is observed for the 30 % and 40 % WG samples. For further investigations into the effect of varying geometric parameters of the breaker plates, SPI was chosen as the protein source.

3.2. Influence of varied hole diameter

To investigate the influence of breaker plates with varying hole diameters on the resulting structure and mechanical properties of the extruded samples, breaker plates with hole diameters of 1 mm, 1.5 mm, and 2 mm were considered. The results for rupture tension in both the transversal and longitudinal directions, as well as the resulting AI of the extruded samples, are shown in Fig. 7. It is evident that rupture tension increases significantly with hole diameter in both the transversal and longitudinal directions and reaches its maximum for extrusion without a breaker plate. Despite the observed increase in transversal rupture tension, the AI decreases with increasing hole diameter from 2.9 to 1.5, which is attributed to comparatively stronger increase in longitudinal than transversal rupture tension. A possible explanation is that the interface between the individual secondary strands acts as a tensile weak point when subjected to orthogonal tensile stress within the extrudate. The magnitude of this interface increases as the hole diameter decreases, for a constant FAR, resulting in a progressively weakened extrudate under longitudinal tensile stress. In contrast, when tensile stress is applied parallel to these interfaces, the number of strands influences the extrudate's strength indirectly by facilitating independent elongation

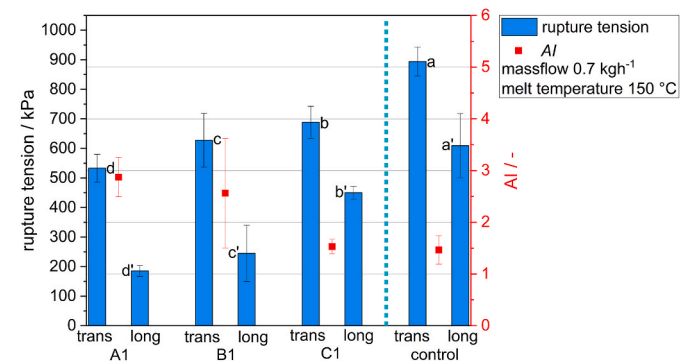


Fig. 7. Rupture tension in transversal and longitudinal direction as well as AI plotted for extrusion with breaker plate of varied hole diameter (A1 = 1 mm; B1 = 1.5 mm; C1 = 2 mm) and a control extruded without breaker plate. Small letters indicate groups with significant differences.

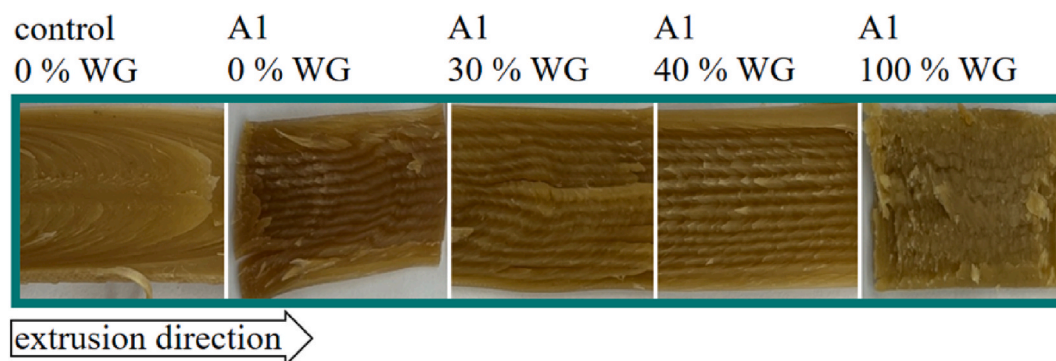


Fig. 6. Torn-open samples from WG-SPI mixtures with varying WG content (0 %, 30 %, 40 %, and 100 %) extruded using breaker plate A1. The control sample on the left with 0 % WG was extruded without a breaker plate. WG content of the depicted samples increases from left to right. All extrudates are oriented in the extrusion direction left to right with an extrudate width of 19 mm.

and rupture of each secondary strand, thereby reducing the maximum rupture tension.

Fig. 8 presents a top view of torn-open extrudates for the different hole diameters of the breaker plate, as well as for the control case, with the extrusion direction oriented from left to right. In the samples shown, a singular parabolic structure is observed, covering the entire flow cross-section. Upon closer inspection, a slight deformation of the singular parabolic shape can be noted, particularly in the center of the cross-section for A1 to C1. This deformation can be attributed to elongational flow at the inflow of each channel, as well as the development of the flow profile within the channels of the breaker plate. Additionally, a secondary structure appears as long, parallel strands in all samples except for the control case. This reinforces the notion from Wittek et al. (Wittek et al., 2021a,b) that primary structure formation primarily occurs in the adapter and cooling die. The control sample also shows a slightly deformed parabolic structure, which also can be seen in the work of Zheng et al. (2024). This can be attributed to the adapter's flow channel transitioning from a twin-circle cross-section to the stadium-shaped cross-section of the cooling die at the end of the screw section.

In the samples A1 and B1 the ruptured surfaces shows clear ups and downs with the strands resulting from the breaker plate. C1 shows a comparatively flat rupture surface. This indicates for C1 that the rupture occurs within the secondary strands rather than in between of them, as it seems to be for A1 and B1. This suggests a stronger inter-strand cohesion for C1 compared to A1 and B1 which is in line with tensile tests in Fig. 7 where the lowest *AI* was seen for C1 among the breaker plates of varied hole size. Therefore, the number of holes can be deduced from the ruptured surface of the extrudates A1 and B1 while for C1 this seems rather difficult.

Deeper insights into the primary and secondary structure gives Fig. 9. On the left side the cryo images can be seen from the front view, for the used breaker plates shown schematically on the right. The cross-sectional area of each strand increases from A1 to C1. With regard to the hole orientation, for A1 three layers of holes stacked while for B1 and C1 only two layers. As indicated with green lines in Fig. 9, for the cross-section this results in a hexagonal shape for the middle strand row of A1. For B1 and C1, a teeth like cross-section can be seen due to two strand rows present. Regarding the primary structure, for all depicted extrudates a structure similar to a multitude of concentric ellipses can be seen. For samples extruded with breaker plate this structure is locally interrupted by the secondary strand interfaces. This suggests, that the primary structure is built in the adapter before the breaker plates. For all extrudates, but especially for C1 a deformation of the concentric ellipse-like shape can be seen, were for each hole concentric cycles seem superposed. This could result from the elongation flow when entering the breaker plate channels. Additionally a development of a laminar flow profile within the secondary strands is to be expected. With exit though the breaker plates, a compressive flow is to be expected diminishing the visible effect of the aforementioned adjacent concentric circular structures.



Fig. 8. Torn-open extrudates from extrusion with breaker plate of varied hole diameter (A1 = 1 mm; B1 = 1.5 mm; C1 = 2 mm) and a control extruded without breaker plate. All extrudates are oriented in the extrusion direction left to right with an extrudate width of 19 mm.

3.3. Influence of varied FAR

It is stated in the literature that elongation flow is one of the major factors influencing structure formation in extruded high-moisture meat analogues (Wittek et al., 2021a,b). To assess the impact of this factor on the mechanical and optical properties when using breaker plates, the number of holes was varied between 10, 12 and 14, while keeping the hole size constant with 2 mm. This results in flow area ratios *FAR* of 0.4, 0.5 and 0.6 for C1 to C3, which leads to an acceleration of flow at the entrance to the breaker plate and thereby increasing the elongation of fluid elements. All other extrusion settings were maintained unchanged. Fig. 10 presents the rupture tension in both transversal and longitudinal directions, as well as the resulting *AI*, for the three breaker plates tested. The results indicate a significant decrease in both transversal and longitudinal rupture tension with increasing *FAR*. Additionally, *AI* increased with rising *FAR* from 1.5 to 6.4, primarily due to a comparatively greater reduction in longitudinal rupture tension than in transversal rupture tension. While it was assumed, that a more pronounced elongation flow due to a decreased *FAR* increases the anisotropy, the opposite could be seen in tensile testing. An explanation could be the facilitated gelation within the breaker plate due to increased residence time for increasing *FAR*, caused by the higher number of holes. Assuming plug flow for a rough estimation of residence time in the breaker plates, Table 2 shows differences of up to 0.16 s between C1 and C3 which corresponds to a rise in residence time of 41 %.

The torn open samples resulting from extrusion with C1, C2 and C3 are given in Fig. 11. For breaker plate C1, with a shorter residence time, rupture seems to occur within the secondary strands, C3 shows rupture between the secondary strands, suggesting a stronger separation between them. For extrusion using breaker plate C2, an intermediate state is observed.

A closer look to the front view of cryo cut extrudates in Fig. 12 reveals a visible difference in the cross view shape of the secondary strands with successive flattening of the teeth-like shape coming from the two layer hole arrangement. Second a reduction in the secondary strand cross section with increasing hole number can be noticed. Regarding the primary structure for all extrudates a deformation of the concentric ellipses can be seen. Other than expected regarding the higher *FAR* and therefore decreased elongation flow before the plates, the primary parabolic shape seems stronger deformed for C3 than C1.

3.4. Influence of varied channel length and mass flow

To investigate the influence of residence time independently from changes in elongation flow, the thickness of the breaker plate was varied from 2 mm to 4 mm, while keeping the *FAR* constant. Additionally, the mass flow rate was varied from 0.7 kg/h to 1.6 kg/h. Assuming a homogenous velocity distribution over the cross section of the breaker plate, a rough estimation can be made for the residence time as shown in Table 3. In accordance to the results obtained from section 3.2, a longer residence time should result in lowered cohesion between the individual strands, resulting in stronger rupture tensions and lower values for the *AI*. In this line of argumentation, increased channel length leads to

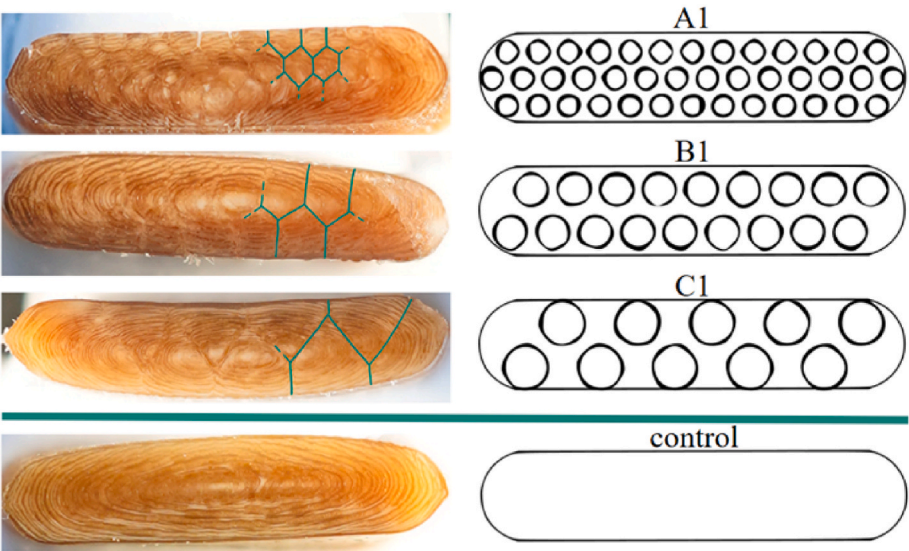


Fig. 9. Front view of cryo cut extrudates for extrusion with breaker plate of varied hole diameter (A1 = 1 mm; B1 = 1.5 mm; C1 = 2 mm) and a control extruded without breaker plate. Green lines schematically indicate the positions of the interfacial boundaries of the individual secondary strands in the front view. The extrudates have a width of 19 mm.

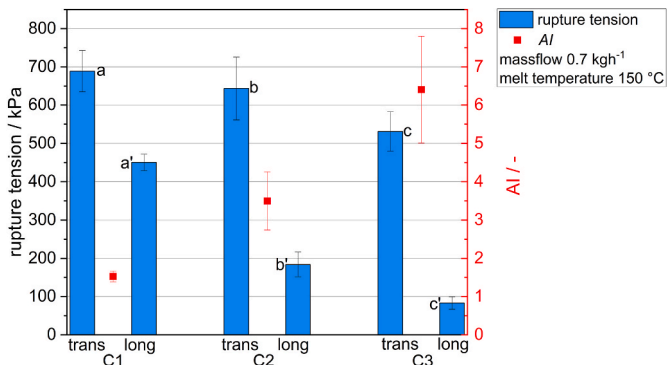


Fig. 10. Rupture tension in transversal and longitudinal direction as well as the AI of the extrudates for extrusion with breaker plate (C1, C2, C3) with varied FAR (0.4, 0.5, 0.6). Small letters indicate groups with significant differences.

Table 2
Estimation of residence time when assuming plug flow for use of C1, C2 and C3 in the extrusion process with mass flows of 0.7 kg/h.

Breaker Plate Geometry	Calculated Residence Time/s
C1	0.39
C2	0.47
C3	0.55

longer a residence time under thermal conditions favorable for gelation processes occur in the flow channels of the breaker plate. For a given inflow and outflow temperature, assuming negligible heat loss to the environment (a reasonable assumption for short plates), the length over which the temperature decreases to the outlet temperature, should increase with longer channels, allowing for gelation to a larger extent inside the breaker plates thereby reducing cohesiveness between the individual strands.

Fig. 13 illustrates the changes in rupture tension in both transversal and longitudinal directions, as well as the resulting AI, for both parameters. It can be observed that an increase in mass flow, and thus reduced residence time, led to significantly higher rupture tensions for both breaker plate configurations. For a constant mass flow of 0.7 kg/h, the increased channel length of breaker plate C3_2 shows reduced values in rupture tension. This further confirms the strength reducing effect of a higher residence time, with a possible explanation lying in the facilitated gel formation within the breaker plates flow channels for increased residence time. However, this conclusion cannot be drawn for a mass flow of 1.6 kg/h, as the transversal rupture tension for C3_2 shows a significantly higher value compared to C3. Whereas for C3, a higher mass flow resulted in a lower AI (reduction from 6.5 to 2.8), this trend was not observed for C3_2, where the AI remained almost unchanged (6.1–6.4). To fully understand the underlying mechanisms, more detailed research is needed regarding flow behavior and the location of gel formation.

The results for optical investigation of the torn-open samples for varied channel length and mass flow are shown in Fig. 14. For breaker plate C3 at a mass flow of 0.7 kg/h, the secondary structure is well-

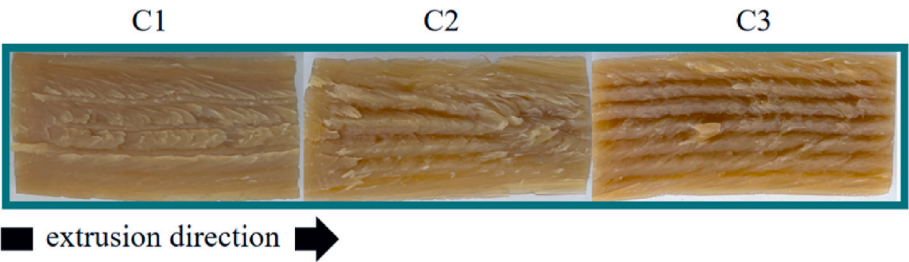


Fig. 11. Torn open extrudates for extrusion with breaker plate (C1, C2 and C3) of varied hole number (10, 12 and 14). All extrudates are oriented in the extrusion direction left to right with the extrudate width being 19 mm.

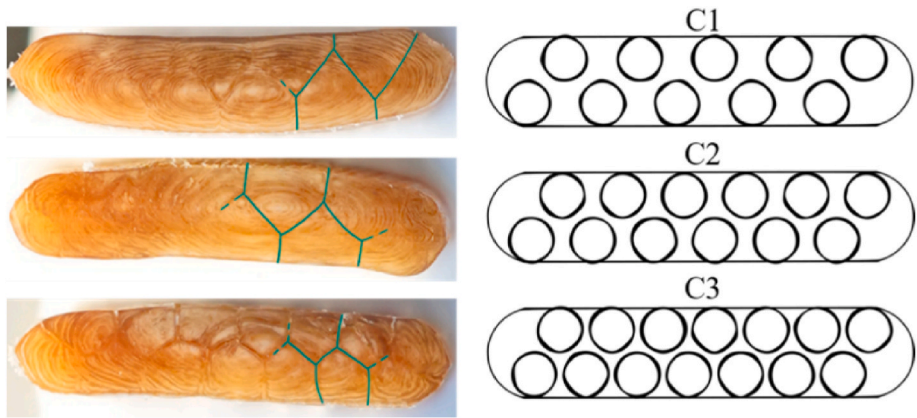


Fig. 12. Front view of cryo cut extrudates for extrusion with breaker plate (C1, C2 and C3) of varied hole number (10, 12 and 14). Green lines schematically indicate the positions of the interfacial boundaries of the individual secondary strands in the front view. The extrudates have a width of 19 mm.

Table 3
Estimation of residence time when assuming plug flow for use of C3 and C3.2 in the extrusion process with mass flows of 0.7 kg/h and 1.6 kg/h.

Breaker Plate Geometry	Mass Flow/kg h ⁻¹	Residence Time/s
C3	0.7	0.55
	1.6	0.24
C3.2	0.7	1.10
	1.6	0.47

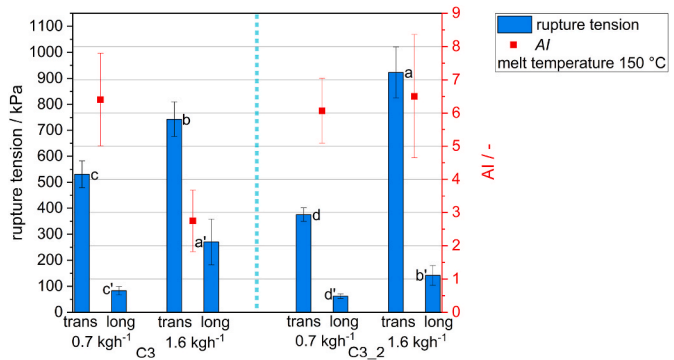


Fig. 13. Rupture tension in transversal and longitudinal direction as well as the AI of the extrudates for extrusion with breaker plate (C3 and C3.2) of varied channel length (2 mm and 4 mm) and two mass flows (0.7 kg/h and 1.6 kg/h). Small letters indicate groups with significant differences.

defined and the rupture seems to occur at the contact surface of the secondary strands. Opposed to that, an increase in mass flow to 1.6 kg/h leads to a partial rupture within the secondary strands, suggesting stronger cohesion between the secondary strands and the dominance of the primary structure. For extrusion with breaker plate C3.2, the

increase in mass flow appears to have little effect on the rupture location, which supports the finding from mechanical testing.

When analyzing the cryo cut samples in Fig. 15, a reduction in the separation between secondary strands with increasing mass flow is noticeable for breaker plate C3. At 1.6 kg/h, the structural influence of the breaker plate is low. In contrast, this effect is not observed for C3.2, where the secondary strands remain clearly distinguishable even at a mass flow of 1.6 kg/h supporting the above results from the tearing.

4. Conclusion

This study explored the impact of extrusion using various breaker plate geometries on the development of fibrous structures on the example of SPI based extrudates for application in processes to produce high-moisture meat analogues. Key geometric parameters, such as hole diameter, hole number, and channel length, were systematically varied. Mechanical analysis and optical methods, such as cryo imaging and visual investigation of torn open samples were employed to assess the resulting structures.

The findings revealed that the use of breaker plates introduced a secondary structure, comprising parallel strands, which overlaid the primary parabolic structure. Importantly, the primary structure was preserved, although minor deformations were observed, likely due to elongational and shear flow effects both before and within the breaker plate. Notably, the achievable anisotropy index (AI) values (spanning 1.5 to 6.5) surpassed those typically obtained in conventional extrusion processes for meat analogues. The geometry of the breaker plate significantly influenced the formation of the secondary structure. Increasing hole diameter led to larger secondary strand cross-sectional areas, which, in turn, reduced the AI (2.9–1.5) due to increased rupture tension perpendicular to the extrusion direction. Furthermore, an increase in the number of holes and, consequently, the flow area ratio altered the shape and size of the secondary strands' cross section. This increase in holes was accompanied by a rise in AI (1.5–6.4), along with a

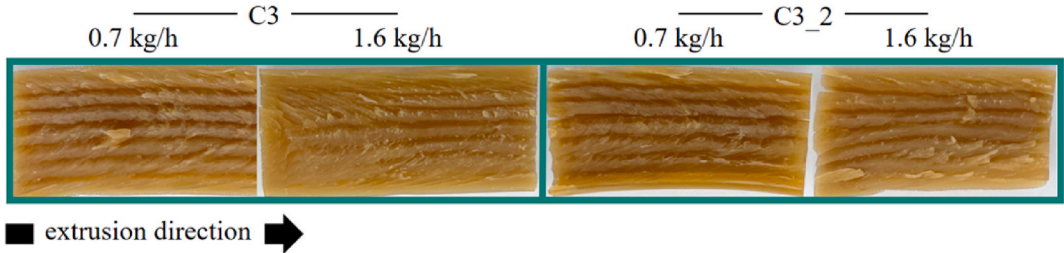


Fig. 14. Torn open extrudates for extrusion with breaker plate (C3 and C3.2) of varied channel length (2 mm and 4 mm) and two mass flows (0.7 kg/h and 1.6 kg/h). All extrudates are oriented in the extrusion direction left to right with the extrudate width being 19 mm.

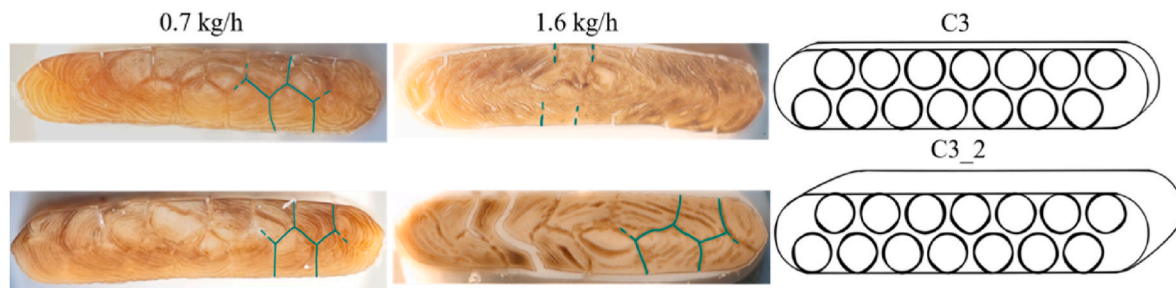


Fig. 15. Cryo cut extrudates for extrusion with breaker plate (C3 and C3_2) of varied channel length (2 mm and 4 mm) and two mass flows (0.7 kg/h and 1.6 kg/h). Green lines schematically indicate the positions of the interfacial boundaries of the individual secondary strands in the front view. The extrudates have a width of 19 mm.

reduction in rupture tension both parallel and perpendicular to the extrusion direction. Increasing the residence time inside the flow channels by increasing breaker plate thickness reduced the sensitivity of both the visually detectable secondary structure and the *AI* to changes in mass flow.

A new structural scale for meat analogues has been introduced, expanding product design possibilities. Analogues with parallel strands could be used to mimic pulled pork or slow-cooked meats. Still more research is needed to further explain underlying mechanisms for structure formation with respect to the influence of flow and gelation conditions.

CRediT authorship contribution statement

Laurids Pernice: Writing – original draft, Methodology, Investigation, Conceptualization. **Désirée Röhrich:** Methodology, Investigation. **Volker Gaukel:** Writing – review & editing. **Nico Leister:** Writing – review & editing, Supervision.

Ethical approval

The conducted research is not related to either human or animal use.

Funding

The research of this work was funded by the Scholarship Program of the Deutsche Bundesstiftung Umwelt.

Declaration of competing interest

The authors declare the following financial interests/personal relationships which may be considered as potential competing interests: Laurids Pernice reports financial support was provided by German Federal Environmental Foundation. If there are other authors, they declare that they have no known competing financial interests or personal relationships that could have appeared to influence the work reported in this paper.

Acknowledgements

We would like to express my gratitude to the Deutsche Bundesstiftung Umwelt (DBU) for providing financial support for this research. A special thanks goes to the Markus Fischer and Jürgen Kraft without whose assistance and expertise the manufacturing of breaker plates wouldn't have been possible. As well we want to thank Kerstin Sauter for her assistance in the extrusion trials.

Appendix A. Supplementary data

Supplementary data to this article can be found online at <https://doi.org/10.1016/j.jfoodeng.2025.112602>.

Data availability

Data will be made available on request.

References

- Akdogan, H., 1999. High moisture food extrusion. *Int. J. Food Sci. Technol.* 34 (3), 195–207. <https://doi.org/10.1046/j.1365-2621.1999.00256.x>.
- Arrigo, R., Malucelli, G., Mantia, F.P.L., 2021. Effect of the elongational flow on the morphology and properties of polymer systems: a brief review. *Polymers* 13 (20), 3529. <https://doi.org/10.3390/polym13203529>.
- Bouvier, J., Campanella, O.H., 2014. *Extrusion Processing Technology: Food and Non-Food Biomaterials* (1. Aufl. Wiley. <https://doi.org/10.1002/9781118541685>.
- Grabowska, K.J., Tekidou, S., Boom, R.M., van der Goot, A.-J., 2014. Shear structuring as a new method to make anisotropic structures from soy-gluten blends. *Food Res. Int.* 64, 743–751. <https://doi.org/10.1016/j.foodres.2014.08.010>.
- Guan, T., Sägeser, C., Villiger, R., Zychowski, L., Kohlbrecher, J., Dümpler, J., Mathys, A., Rühls, P., Fischer, P., Matsarskaia, O., 2024. In situ studies of plant-based meat analog texturization. *Food Hydrocoll.* 155, 110215. <https://doi.org/10.1016/j.foodhyd.2024.110215>.
- Hoek, A.C., Luning, P.A., Weijzen, P., Engels, W., Kok, F.J., Graaf, C., 2011. Replacement of meat by meat substitutes. A survey on person- and product-related factors in consumer acceptance. *Appetite* 56 (3), 662–673. <https://doi.org/10.1016/j.appet.2011.02.001>.
- IPCC, 2023. *Climate Change 2022 – Impacts, Adaptation and Vulnerability*. Cambridge University Press. <https://doi.org/10.1017/9781009325844>.
- Jiang, L., Zhang, H., Zhang, J., Liu, S., Tian, Y., Cheng, T., Guo, Z., Wang, Z., 2024. Improve the fiber structure and texture properties of plant-based meat analogues by adjusting the ratio of soy protein isolate (SPI) to wheat gluten (WG). *Food Chem. X* 24, 101962. <https://doi.org/10.1016/j.fochx.2024.101962>.
- Kaunisto, E., Wassén, S., Stading, M., 2024. A thermodynamical finite element model of the fibre formation process during extrusion of high-moisture meat analogues. *J. Food Eng.* 362, 111760. <https://doi.org/10.1016/j.jfoodeng.2023.111760>.
- Köllmann, N., Schreuders, F.K.G., Zhang, L., Van Der Goot, A.J., 2023. On the importance of cooling in structuring processes for meat analogues. *J. Food Eng.* 350, 111490. <https://doi.org/10.1016/j.jfoodeng.2023.111490>.
- Krintiras, G.A., Göbel, J., Van Der Goot, A.J., Stefanidis, G.D., 2015. Production of structured soy-based meat analogues using simple shear and heat in a Couette Cell. *J. Food Eng.* 160, 34–41. <https://doi.org/10.1016/j.jfoodeng.2015.02.015>.
- Lee, S.Y., Lee, D.Y., Jeong, J.W., Kim, J.H., Yun, S.H., Joo, S.-T., Choi, I., Choi, J.S., Kim, G.-D., Hur, S.J., 2023. Studies on meat alternatives with a focus on structuring technologies. *Food Bioprocess Technol.* 16 (7), 1389–1412. <https://doi.org/10.1007/s11947-022-02992-0>.
- Leland, M., Trigg, A., Kim, Y.H.B., 2022. Meat analogues: an assessment of plant-based protein options and the parameters of their success: a mini review. *Food and Life* 2022 (2), 51–57. <https://doi.org/10.5851/fl.2022.e8>.
- Mateen, A., Mathpati, M., Singh, G., 2023. A study on high moisture extrusion for making whole cut meat analogue: characterization of system, process and product parameters. *Innov. Food Sci. Emerg. Technol.* 85, 103315. <https://doi.org/10.1016/j.ifset.2023.103315>.
- Osen, R., Toelstede, S., Wild, F., Eisner, P., Schweiggert-Weisz, U., 2014. High moisture extrusion cooking of pea protein isolates: raw material characteristics, extruder responses, and texture properties. *J. Food Eng.* 127, 67–74. <https://doi.org/10.1016/j.jfoodeng.2013.11.023>.
- Parlasca, M.C., Qaim, M., 2022. Meat Consumption and Sustainability. *Ann. Rev. Resour. Econ.* 14 (1), 17–41. <https://doi.org/10.1146/annurev-resource-111820-032340>.
- Pematilleke, N., Kaur, M., Adhikari, B., Torley, P.J., 2022. Relationship between instrumental and sensory texture profile of beef *semitendinosus* muscles with different textures. *J. Texture Stud.* 53 (2), 232–241. <https://doi.org/10.1111/jtxs.12623>.
- Pibarot, P., Schmitt, C.J.E., Sanchez, C., Morel, M.-H., Université de Montpellier, I.N. de la R.A., 2020. *Meat Analogues and Meat Analogue Extrusion Devices and Methods*. Sägeser, C., Mair, T., Braun, A., Dümpler, J., Fischer, P., Mathys, A., 2025. Application of a shear cell for the simulation of extrusion to test the structurability of raw materials. *Food Hydrocoll.* 160, 110736. <https://doi.org/10.1016/j.foodhyd.2024.110736>.

- Sakellarides, S.L., McHugh, A.J., 1987. Structure formation during polymer blend flows. *Polym. Eng. Sci.* 27 (22), 1662–1674. <https://doi.org/10.1002/pen.760272204>.
- Sandoval Murillo, J.L., Osen, R., Hiermaier, S., Ganzenmüller, G., 2019. Towards understanding the mechanism of fibrous texture formation during high-moisture extrusion of meat substitutes. *J. Food Eng.* 242, 8–20. <https://doi.org/10.1016/j.jfoodeng.2018.08.009>.
- Sengar, A.S., Beyrer, M., McDonagh, C., Tiwari, U., Pathania, S., 2023. Effect of process variables and ingredients on controlled protein network creation in high-moisture plant-based meat alternatives. *Foods* 12 (20), 3830. <https://doi.org/10.3390/foods12203830>.
- Snel, S.J.E., Bellwald, Y., van der Goot, A.J., Beyrer, M., 2022. Novel rotating die coupled to a twin-screw extruder as a new route to produce meat analogues with soy, pea and gluten. *Food Hydrocoll.* 81 (May), 103152. <https://doi.org/10.1016/j.ifset.2022.103152>.
- Tolstoguzov, V.B., 1993. Thermoplastic extrusion—the mechanism of the formation of extrudate structure and properties. *JAOCS (J. Am. Oil Chem. Soc.)* 70 (4), 417–424. <https://doi.org/10.1007/BF02552717>.
- van der Sman, R.G.M., van der Goot, A.J., 2023. Hypotheses concerning structuring of extruded meat analogs. *Curr. Res. Food Sci.* 6, 100510. <https://doi.org/10.1016/j.crfs.2023.100510>.
- Wagner, C.E., Levine, L., Saunders, S.R., Bergman, R., Guo, X., Ganjyal, G.M., 2024. The impact of temperature gradient, apparent shear rate, and inferred phase transition timing on extruded high moisture meat analog quality. *Food Res. Int.* 192, 114760. <https://doi.org/10.1016/j.foodres.2024.114760>.
- Wittek, P., Ellwanger, F., Karbstein, H.P., Emin, M.A., 2021a. Morphology development and flow characteristics during high moisture extrusion of a plant-based meat analogue. *Foods* 10 (8). <https://doi.org/10.3390/foods10081753>.
- Wittek, P., Zeiler, N., Karbstein, H.P., Emin, M.A., 2021b. High moisture extrusion of soy protein: investigations on the formation of anisotropic product structure. *Foods* 10 (1). <https://doi.org/10.3390/foods10010102>.
- Zheng, Y., Xu, J., Sun, C., Zhao, Y., Cao, Y., Lu, W., Zhang, Y., Fang, Y., 2024. Multihole nozzle-mediated high-moisture extrusion of soy proteins into fiber-rich structures. *Food Hydrocoll.* 151 (3), 109819. <https://doi.org/10.1016/j.foodhyd.2024.109819>.
- Zink, J.I., Zeneli, L., Windhab, E.J., 2023. Micro-foaming of plant protein based meat analogues for tailored textural properties. *Curr. Res. Food Sci.* 7, 100580. <https://doi.org/10.1016/j.crfs.2023.100580>.